Original Article

Evaluation of Asymmetry in Right and Left Eyes of Normal Individuals Using Extracted Features from Optical Coherence Tomography and Fundus Images

Tahereh Mahmudi[1,2], Raheleh Kafieh[1], Hossein Rabbani[1], Alireza Mehri[1], Mohammad-Reza Akhlaghi[3]

[1]Department of Medical Physics and Biomedical Engineering, School of Medicine, Tehran University of Medical Sciences, Tehran, [2]Medical Image and Signal Processing Research Center, School of Advanced Technologies in Medicine, Isfahan University of Medical Sciences, [3]Department of Ophthalmology, School of Medicine, Isfahan University of Medical Sciences, Isfahan, Iran

Abstract

Background: Asymmetry analysis of retinal layers in right and left eyes can be a valuable tool for early diagnoses of retinal diseases. To determine the limits of the normal interocular asymmetry in retinal layers around macula, thickness measurements are obtained with optical coherence tomography (OCT). **Methods:** For this purpose, after segmentation of intraretinal layer in threedimensional OCT data and calculating the midmacular point, the TM of each layer is obtained in 9 sectors in concentric circles around the macula. To compare corresponding sectors in the right and left eyes, the TMs of the left and right images are registered by alignment of retinal raphe (i.e. diskfovea axes). Since the retinal raphe of macular OCTs is not calculable due to limited region size, the TMs are registered by first aligning corresponding retinal raphe of fundus images and then registration of the OCTs to aligned fundus images. To analyze the asymmetry in each retinal layer, the mean and standard deviation of thickness in 9 sectors of 11 layers are calculated in 50 normal individuals. **Results:** The results demonstrate that some sectors of retinal layers have signifcant asymmetry with $P < 0.05$ in normal population. In this base, the tolerance limits for normal individuals are calculated. **Conclusion:** This article shows that normal population does not have identical retinal information in both eyes, and without considering this reality, normal asymmetry in information gathered from both eyes might be interpreted as retinal disorders.

Keywords: *Alignment, asymmetry analysis, fundus images, optical coherence tomography*

Submitted: 14-Dec-2019 **Revision:** 14-Feb-2020 **Accepted:** 09-Mar-2020 **Published:** 30-Jan-2021

Introduction

Recently, optical coherence tomography (OCT) has revolutionized the clinical imaging of the retina by a noninvasive imaging modality in the diagnosis of ocular diseases.[1,2] The high-resolution, cross-sectional images of the retina can be obtained by OCT systems, and it provides a valuable tool for measuring the parameters of retinal morphology.[3] Improvements in automatic analysis will be beneficial to clinicians as it can improve the speed and accuracy of their diagnoses. Therefore, the automatic extraction of parameters such as retinal layer thickness is already possible.

Asymmetry analysis is a valuable tool for early diagnoses of retinal diseases. For instance, it is very common to investigate glaucomatous eyes by visual field tests. However, such a test is not sensitive enough to find very small loss in layers such as ganglion cells. By only focusing on interindividual variations in one eye, such small losses may not be found. This can simply justify our need to consider interocular differences to compare thicknesses of two eyes from one individual. It is expected that small interocular differences (compared to variation across individuals) in normative database would provide an asymmetry limit range for normal population. It is also expected that different diseases would alter the symmetry to fall outside the normative range. This is already shown in symmetry analysis of retinal nerve fiber layer (RNFL) in glaucoma,[4] but more sophisticated diseases affecting other retinal layers may also be considered.

For asymmetry analysis in retinal images, a number of previous works

How to cite this article: Mahmudi T, Kafieh R, Rabbani H, Mehri A, Akhlaghi MR. Evaluation of asymmetry in right and left eyes of normal individuals using extracted features from optical coherence tomography and fundus images. J Med Sign Sens 2021;11:12-23.

Address for correspondence:
Dr. Raheleh Kafieh, Medical Image and Signal Processing Research Center, School of Advanced Technologies in Medicine, Isfahan University of Medical Sciences, Isfahan, Iran.
E-mail: rkafieh@gmail.com

Access this article online

Website: www.jmssjournal.net

DOI: 10.4103/jmss.JMSS_67_19

Quick Response Code:

are available.[4-25] For instance, interocular symmetry/asymmetry was analyzed on the RNFL thickness (RNFLT) of the retina on OCT images in normal population to discriminate normal/abnormal cases. Table 1 summarizes the available works on symmetry of retinal layers between the right and left eyes using OCT.

To the best of our knowledge, no study is undertaken to evaluate symmetry of all 11 subretinal layers in concentric circles around the macula, by standards of the Early Treatment Diabetic Retinopathy Study (ETDRS) in normal population, and the presented work determines that the normal tolerance limit is each sector of the mentioned circles for all 11 subretinal layers.

The purpose of this study is to determine normal tolerance limits for asymmetry of retinal layer thickness between two eyes and to infer that measurements beyond this level are signature of possible abnormalities. This article is extension of Mahmudi *et al*.'s study;[17] compared to which the number of volunteers is increased from 19 to 50, the evaluated layers consist 11 intraretinal layers rather than only focusing on RNFL and total retinal thickness, and the right and left eyes are aligned according to retinal raphe using a combined method by means of registration,[26] alignment, and fusion to provide a correct comparison.

Materials and Methods

Materials

The set of images is provided by the Ophthalmology Department, Feiz Hospital, Isfahan, Iran. The Ethics Committee of Isfahan University of Medical Sciences approved the study protocol, and the individuals gave approval before inclusion and provided written informed consent. Fifty normal individuals (age 45 ± 10 years) participated in this study and underwent a comprehensive test; two eyes of each patient were tested with three-dimensional (3D) OCT-1000 (MK2, Ver. 3.51) Topcon device which could produce both fundus and OCT images. The inclusion criteria for normal eye are presented in Table 2.

The individuals were recruited by advertisement among the general population of students and staff in the Department of Advanced Technologies in Medicine, Isfahan University of Medical Sciences, Isfahan, Iran.

Each captured image includes two modalities of OCT data and fundus image (described below):

Optical coherence tomography data

Each data includes macular OCTs of the right and left eyes. The dimension of the OCT data is 650 × 512 × 128 voxels with a voxel resolution of 3.54 × 11.72 × 46.88 μm which correspond to axial, nasal-temporal, and superior-inferior orientations. The dataset is, therefore, composed of 128 slices with a size of 650 × 512.

Fundus images

Each image includes two-color fundus image of the retina from the left and right eyes with dimension of 1534 ×1612 pixels.

The dataset is publicly available in https://sites.google.com/site/hosseinrabbanikhorasgani/datasets-1/

Table 1: Studies on symmetry of retinal layers between the right and left eyes using optical coherence tomography

Research	Publication year	Retinal layers	Tolerance limit calculation (yes/no)	Population	OCT type	Sector analysis (yes/no)
Kurimoto *et al*.[6]	2000	RNFL	No	Normal	ONH	PRNFL
Park *et al*.[9]	2005	RNFL	No	Normal	ONH	PRNFL
Budenz[10]	2008	RNFL	Yes	Normal	ONH	PRNFL
Asrani *et al*.[4]	2011	RNFL	No	Normal	Macula	Posterior pole grid
Larsson *et al*.[11]	2011	RNFL	Yes	Normal	ONH	PRNFL
Altemiret al.[12]	2013	RNFL	Yes	Normal	Macula	ETDRS
Dalgliesh *et al*.[14]	2015	RNFL	No	Normal	Macula	ETDRS
Al-Haddad *et al*.[13]	2014	RNFL	No	Normal	Macula	ETDRS
Alluwimi *et al*.[15]	2014	RNFL	No	Normal	Macula	Posterior pole grid
Hwang *et al*.[18]	2014	RNFL	Yes	Normal	Macula	ETDRS
Lee *et al*.[19]	2015	GCL	Yes	Normal, glaucoma patients	Macula	No
Dalgliesh *et al*.[20]	2015	RNFL, total macula	Yes	Normal	Macula	ETDRS
Zhou *et al*.[21]	2016	GCL	No	Normal	Macula	ETDRS
Yang *et al*.[22]	2016	RNFL, PCT, SFCT	Yes	Isometropia patients	EDI OCT	ETDRS
Lee *et al*.[23]	2016	RNGL, GCIPL, ganglion cell complex, total retina	No	Normal, glaucoma patients	Macula	No
Yamada *et al*.[24]	2014	RNFL, GCL, ganglion cell complex, total retina	Yes	Normal, preperimetric, early, and advance glaucoma	Macula	Upper and lower hemi retinal

RNFL – Retinal nerve fiber layer; PRNFL – Peripapillary RNFL; OCT – Optical coherence tomography; GCL – Ganglion cell layer; PCT – Peripapillary choroidal thickness; SFCT – Subfoveal choroidal thickness; ONH – Optic nerve head; EDI – Enhanced depth imaging; ETDRS – Early Treatment Diabetic Retinopathy Study; GCIPL – Ganglion cell and inner plexiform layer

oct-fundus-right-left and https://hrabbani.site123.me/available-datasets/oct-data-color-fundus-images-of-left-right-eyes-of-50-healthy-persons.

Asymmetry analysis for thickness of retinal layers

Covering a great part of the eye, the retina is a multilayered structure responsible for transforming light into neural signals for further use by the brain. In this article, using automatic 3D segmentation on each dataset,[27] thickness maps (TMs) of 11 retinal layers in OCT, pertaining to histological retinal layers, were generated.

- Layer 1: nerve fiber layer
- Layer 2: ganglion cell layer
- Layer 3: inner plexiform layer
- Layer 4: inner nuclear layer
- Layer 5: outer plexiform layer
- Layer 6: outer nuclear layer
- Layer 7: inner segment layer
- Layer 8: connecting cilia
- Layer 9: outer segment layer
- Layer 10: Verhoeff membrane
- Layer 11: retinal pigment epithelium (RPE), also called the vitreous lamina.[28]

The proposed method compares each layer in two eyes of an individual and looks for tolerance limits of normal eyes. For this purpose, different steps are proposed, as demonstrated in Figure 1. The 3D segmentation is needed for calculation of each boundary; however, the OCTs in the right and left eyes need to have identical rotation to have a correct comparison in the right and left eyes. That is why the next steps are proposed to find the retinal raphe and to correct the rotation. Construction of OCT projection, determination of macular center, construction of TM, and finally registration are the steps for retinal raphe alignment. Finally, the registered TMs are analyzed in 9 sectors of concentric circles to determine the asymmetry of the left and right eyes and to find the tolerance limits for each sector in each layer. Each step of the block diagram in Figure 1 is elaborated in the following subsections.

Table 2: Inclusion criteria for normal eye

1. No history or evidence of systemic diseases (diabetes mellitus, severe or uncontrolled systemic hypertension, pregnancy, cancer, kidney transplant, and autoimmune disease) or ophthalmic diseases (amblyopia, high intraocular pressure (IOP>21 mmHg), glaucoma and previous ocular surgery, macular degeneration, hazy media), or poor cooperation, which prevents high-quality image acquisition
2. Visual acuity over 0.6
3. Spherical equivalent on refraction of within±3.0 diopters
4. Intraocular pressure <21 mmHg
5. Cup-disc ratio <0.6 (measured by OCT)

IOP – Intraocular pressure; OCT – Optical coherence tomography

Segmentation using diffusion map method

In this study, we used 3D intraretinal layer segmentation algorithm (using coarse-grained diffusion map)[27] on spectral-domain OCTs. This method is a fast segmentation method based on a spectral graph method named diffusion maps.[29-31] In contrast to other methods of graph-based OCT image segmentation, the presented approach does not require edge-based image information and rather relies on regional image texture.[32] As described in detail in Kafieh *et al.*'s study,[27] the method demonstrates robustness in low image contrast and poor layer-to-layer image gradients.

Each two-dimensional (2D)/3D OCT image was analyzed to localize 11 layers (12 surfaces), as shown in Figure 2. Signed and unsigned errors of the method in Kafieh *et al.*'s study[27] (according to independent standard resulted from averaging tracings from two expert observers) are 8.52 ± 3.13 and 7.56 ± 2.95 μm, respectively.

Optical coherence tomography projection and scaling

It is possible to collapse 3D OCT volumes along the depth axis to make a 2D projection map. There are several methods for making a projection such as averaging, highest, or lowest values of each column of 3D space.[33,34]

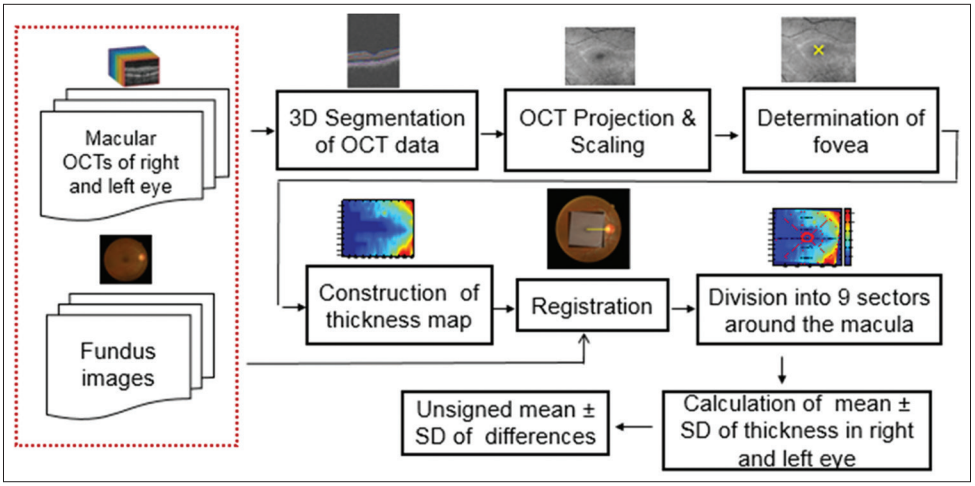

Figure 1: Functional block diagram for asymmetry analysis of retinal layers

In this study, we used the column average of 3D OCT slices to create a projection demonstrated in Figure 3. Such a projection image demonstrated a clear macular region, but the vessels are not obvious enough for vessel segmentation. Therefore, a limited averaging along x-axis is proposed in outer retinal layers to produce vessel maps with clear vessel information.[35] This map, however, is not a good indicator for the macula region.

One important consideration in sampling ratio between OCT slices and corresponding fundus image is a four-time scaling in vertical axes. The size of each projection is 128 × 512 with a resolution of 46.88 × 11.72 μm/pixel. It can be simply seen that the vertical resolution is four times higher than horizontal resolution, and we can change the size of each projected image into 512 × 512 by scaling of vertical pixels and achieving equal resolution of 11.72 μm/pixel as shown in Figure 4.

Determination of the macular center (fovea) in optical coherence tomography projections for ETRDS step

A diverse collection of methods is already proposed for automatic localization of fovea.[36-39] We propose a simple strategy to find the middle point of the macula by pattern-matching scheme. First of all, we made 10 training templates (sized 153 × 153) manually located at the center of the macula. The averaged version of these templates was used as final template. Then, we used 2D convolution on averaged template and target image. Using maximum value, the coordinate of the center of macula was selected as the center point, as shown in Figure 5. For validation purpose, we compared the results with manual labeling of macula and 20.51 ± 6.09 μm error was achieved.

Construction of the thickness map

Analysis of thickness in retinal layers is an important way to quantify pathological changes.[40] In this study, the TMs are calculated by subtracting the location of two consequent boundaries calculated by 3D segmentation.[32] The boundaries first went into a curvature correction step with reference to lower boundary of RPE and are flattened before calculation of the thickness values.[32,41] The flattening step removes the tilt in B-scans which may be due to off-axis image acquisition, and since the curvature correction is performed in both the right and left eyes, the tilt angle will be removed similarly in both eyes.[42] TMs of the 11 retinal layers in the right and left eyes are displayed in pseudo color [Figure 6a-k]. Total retinal layer thickness

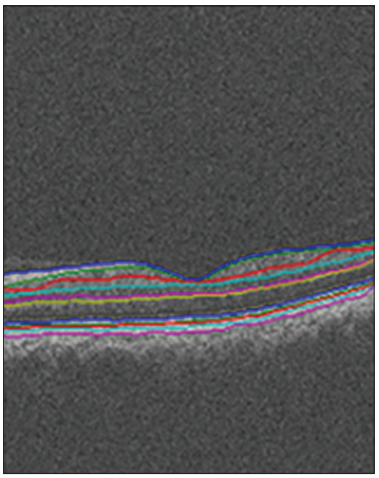

Figure 2: Segmentation results of one slice from a 650 × 512 × 128 spectral-domain optical coherence tomography

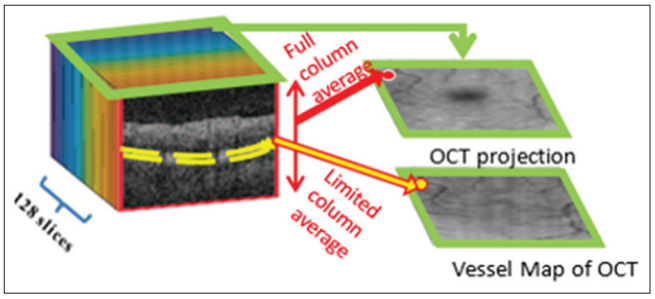

Figure 3: Optical coherence tomography projection image generated by averaging each A-scan contains macular location, but vessel information is unclear. The vessel map of optical coherence tomography is then generated by averaging outer retinal layers (after segmentation) to make clear vessel information without clear region

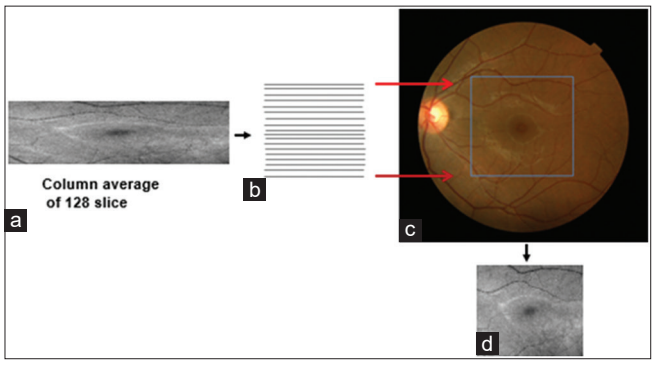

Figure 4: (a) Optical coherence tomography projection, (b) Looking for proper interpolation to compensate the difference of vertical and horizontal resolutions, (c) Mutual correspondence between optical coherence tomography and fundus data, (d) interpolated optical coherence tomography projection

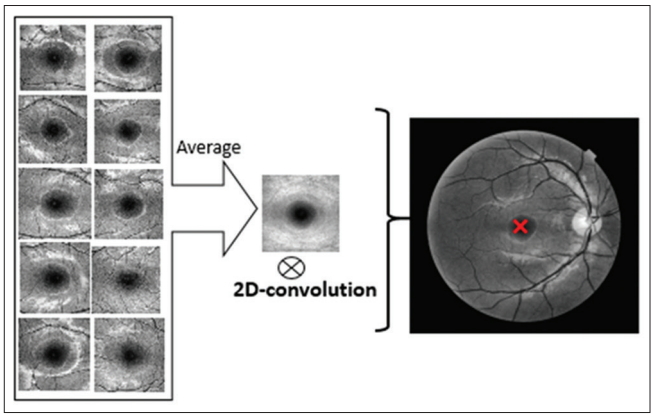

Figure 5: Two-dimensional convolution of the averaged templates with the original image to find the center of the macula

is also calculated by summing thickness measurements in 11 layers [Figure 6l].

Registration

As described above, the OCTs in the right and left eyes should have identical rotation to provide a correct comparison in the right and left eyes. The axons of retina pass over a route to optic nerve head (ONH) without passing from the fovea (raphe). The correct location of raphe discriminates superior and inferior regions correctly, and the overlaid ETRDS lines match the OCT data. However, if the raphe would not be correctly located, the ETRDS sectors will mix the OCT information, and the thickness values would be incorrect. Furthermore, the locations in the right and left eyes will not correspond mutually. Even, if we assume that raphe orientation would be identical in both eyes, we need this alignment due to the need for being registered with other individuals.

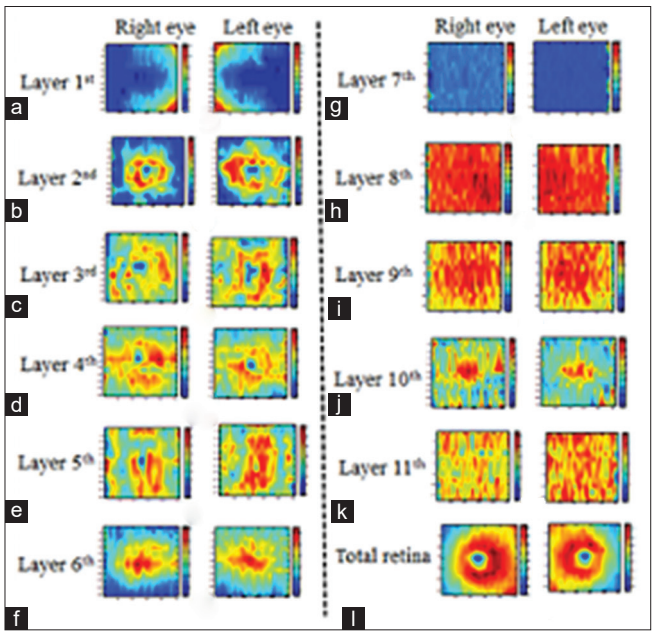

Figure 6: Thickness maps obtained from 11 retina layers (6a-k) and total retina (6l) in the left and right eyes of one participant

One way for making identical rotation in both eyes is alignment based on retinal raphe (in this article, estimated by the line connecting macula to ONH); however, ONH is not detectable in projection images from macular OCTs. Therefore, the proposed strategy is to align the accompanying fundus images of the right and left eyes according to retinal raphe and then to register each OCT to the corresponding fundus image using extracted vessels in both modalities. Figure 7 shows the proposed alignment and registration method, and each step is elaborated in more detail in the next subsections.

Alignment of the accompanying fundus images

We used the retinal raphe for aligning fundus images of both eyes by rotating each fundus image to horizontal retinal raphe [Figure 8]. To obtain the retinal raphe, middle point of the macula and optic disc in fundus image were obtained using a pattern-matching scheme by manual building of 10 training templates located at the center of the macula and ONH. The size of the macular templates is chosen (empirically) to be 201 × 201, and the size of the ONH templates is chosen to be 121 × 121. Then, an averaged version of these

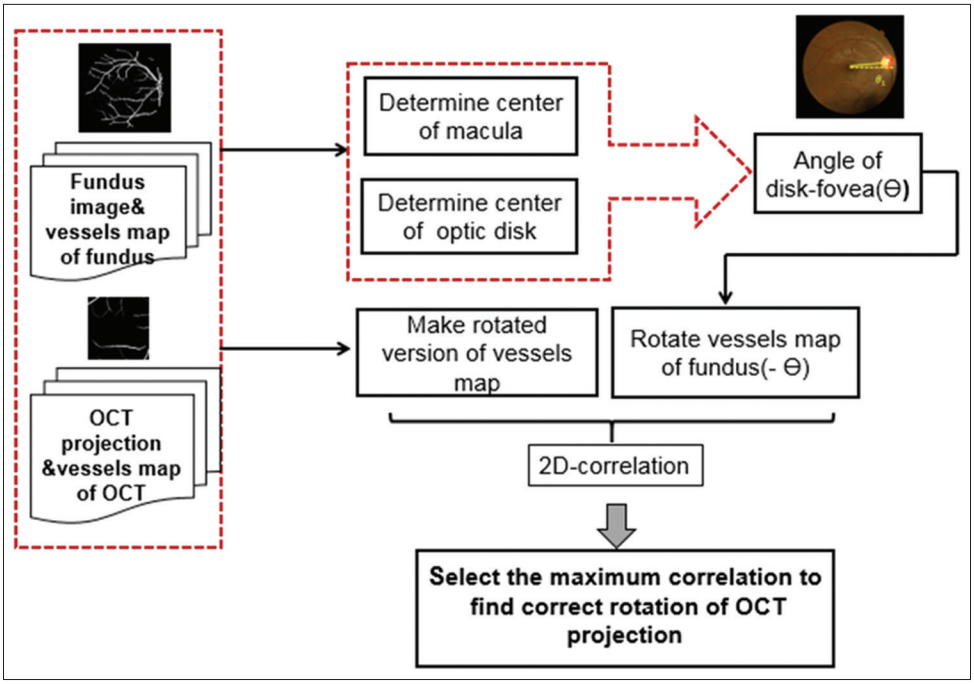

Figure 7: Functional block diagram of the proposed method for alignment of the accompanying fundus images of the right and left eyes according to retinal raphe and then registration of each optical coherence tomography projection to corresponding fundus image using extracted vessels

templates was used as the final template to be used in 2D convolution [Figure 9]. It should be mentioned that the proposed pattern-matching method for localization of optic disc or fovea may only be valid in normal individuals (which are of our interest in this article); however, if the proposed method would be applied on a population with unknown ocular condition, we may need to substitute the simple pattern-matching method with more complex methods like.[43,44]

Registration of each optical coherence tomography to corresponding fundus image using extracted vessels

In this step, we have the correctly aligned fundus images, and if we register each OCT image with its corresponding fundus image, all four versions in the right and left eyes will have identical information. Since the OCT projection and fundus images vary in brightness and grayscale information, the main reliable information for registration of these two modalities is the extracted vessels. We chose an accurate vessel extraction method[45] for both modalities, as shown in Figure 10.

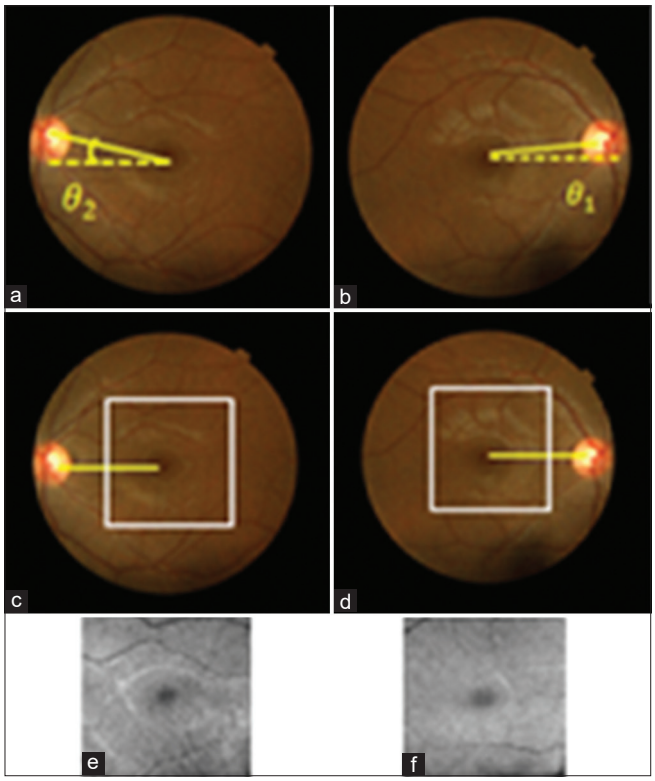

Figure 8: (a and b) Fundus images before alignment, (c and d) Fundus image after alignment with the specified area of optical coherence tomography projection, (e and f) corresponding optical coherence tomography projections

For registration of vessels in two modalities, we used 2D correlation between the aligned fundus data (with horizontal retinal raphe) and different versions of OCT data, rotated from −15 to 15 degrees [Figure 11]. The correlation value was found for each rotated OCT, and the maximum answer was selected as the "best rotation." The calculated "best rotation" is then applied on 11 TMs derived from different layers of OCT, and the reported results were calculated according to these new registered versions.

Division into nine sectors around the macula

To quantify the results, the mean thickness of each retinal layer was investigated by allocating three concentric circles based on the ETDRS standard grid with diameters of 1, 3, and 6 mm in 4 quadrants and 9 sectors around the macula[46] [Figure 12]. The mean ± standard deviation (SD) of pixels in each sector was calculated.

The purpose of this study is to determine the tolerance limits for asymmetry of retinal layer thickness on normal populations. Using these tolerance limits, one may obtain a criterion for the diagnosis of particular diseases. For this purpose, at first, we obtained a mean difference (right thickness minus left thickness) in each layer. The center of macula defines the center of the concentric circles. The central circle represents the central foveal area; the second circle was subdivided into temporal/nasal (sector 2), inferior (sector 3), nasal/temporal (sector 4), and superior (sector 5) parafoveal retinal areas for the left/right eye. The third circle is similarly subdivided into temporal/nasal (sector 6), inferior (sector 7), nasal/temporal (sector 8), and superior (sector 9) perifoveal retinal areas for the left/right eye. Note that in the right and left eyes, the labels 3, 5, 7, and 9 are mirrored. For each

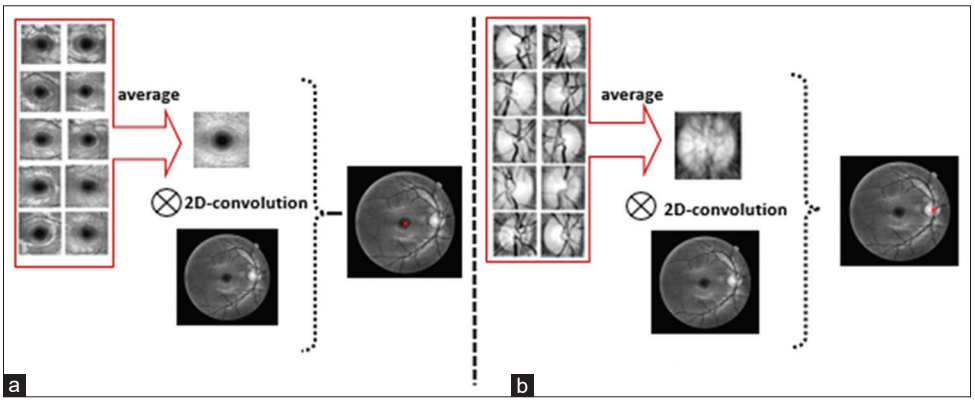

Figure 9: Two-dimensional convolution of the averaged templates with the original fundus image to find the (a) center of the macula, (b) center of the optic disk

of 9 sectors, and for each of 11 layers, the mean and SD of thickness are calculated by taking the average and SD from all 50 3D datasets. Total retinal layer thickness is also calculated for each sector, by summing the thickness of all 11 layers. A sample of such rotated version of the TM for the first layer (RNFL) with ETDRS grid is demonstrated in Figure 13. Furthermore, Figure 14 shows all four versions (OCT TM and fundus in both eyes) with ETDRS grid after registration.

The next step to evaluate the asymmetry between the right and left eyes is calculating mean thickness difference (right thickness minus left thickness) in each layer. To justify the significance of the obtained differences, we also reported the corresponding *P* values.

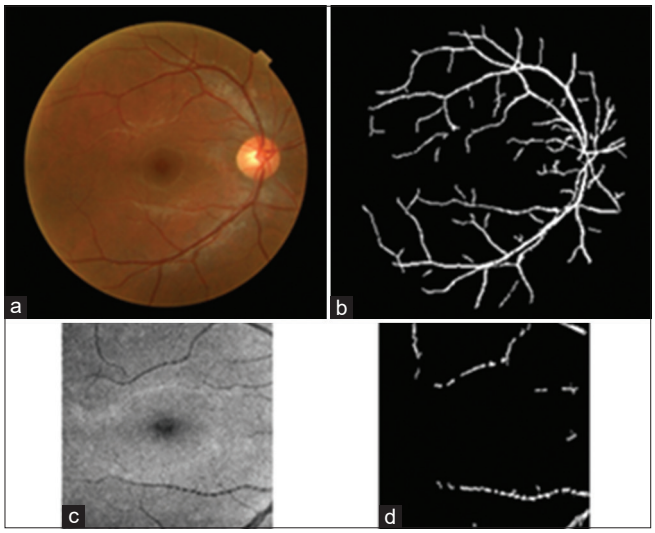

Figure 10: (a) Original fundus image, (b) segmented vessels, (c) corresponding optical coherence tomography projection, (d) segmented vessels

Statistical analysis

Data were analyzed using MATLAB software, version 2012 (Mathworks, Natick, Mass). The Student's *t*-test was used to compare independent groups' averaged differences. Continuous variables are presented as mean ± SD. A two-sided $P < 0.05$ was considered statistically significant. In order to have a quantitative measure of the symmetry between the right and left eyes, the mean thickness difference (right thickness minus left thickness) in each layer is investigated for 9 sectors around the macula. For diagnostic parameters (following a Gaussian distribution) in the healthy population, the mean ± twice the SD was calculated to contain 95% normal limits[10]

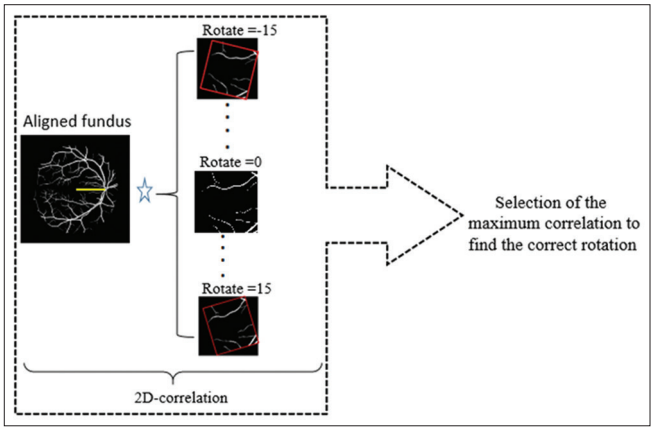

Figure 11: Two-dimensional correlation between aligned fundus (with horizontal retinal raphe) and rotated optical coherence tomography projections

Table 3: The maximum and minimum of the thickness for each layer

Layers	The maximum of thickness/sector (right eye) - The maximum of thickness/sector (left eye)	The minimum of thickness/sector (right eye) - The minimum of thickness/sector (left eye)
1th layer (RNFL)	39.35±11.95/perifoveal nasal - 38.03±11.07/perifoveal nasal	9.96±1.33/fovea - 10.75±0.75/fovea
2nd layer	61.66±13.76/parafoveal temporal - 59.66±12.56/parafoveal temporal	18.06±9.27/fovea - 18.59±9.75/fovea
3rd layer	39.14±7.04/parafoveal nasal - 40.73±7.02/parafoveal nasal	17.90±7.85/fovea - 19.19±7.31/fovea
4th layer	46.13±7.01/parafoveal nasal - 46.35±6.58/parafoveal inferior	36.07±7.03/fovea - 33.45±7.11/fovea
5th layer	20.50±4.34/perifoveal superior - 20.34±4.70/perifoveal superior	2.97±0.99/fovea - 11.89±4.02/fovea
6th layer	78.79±6.04/fovea - 81.08±4.90/fovea	56.18±9.76/perifoveal inferior - 58.07±10.82/perifoveal inferior
7th layer	29.74±2.62/parafoveal temporal - 28.29±0.85/parafoveal temporal	27.48±2.24/fovea - 27.11±1.42/fovea
8th layer	17.19±1.158/parafoveal nasal - 17.21±1.22/fovea	15.57±2.87/perifoveal temporal - 16.02±2.08/perifoveal inferior
9th layer	11.58±0.77/fovea - 11.64±0.80/fovea	9.40±1.79/perifoveal temporal - 9.43±1.52/perifoveal inferior
10th layer	16.81±1.55/fovea - 16.86±1.56/fovea	11.13±2.58/perifoveal temporal - 11.08±1.84/perifoveal superior
11th layer	26.81±3.25/perifoveal superior - 27.12±3.34/perifoveal superior	25.16±2.51/parafoveal temporal - 25.23±2.26/parafoveal temporal
Total retina thickness	337.67±16.92/parafoveal superior - 339.59±16.09/parafoveal superior	270.99±18.14/fovea - 275.929±17.80/fovea

RNFL – Retinal nerve fiber layer

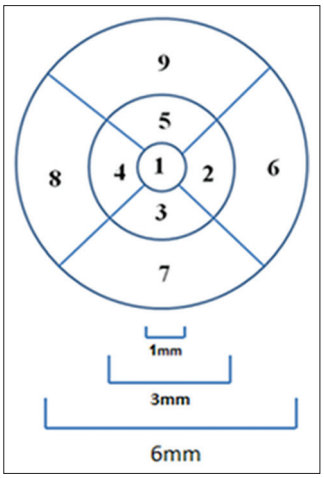

Figure 12: Circle scanning areas (diameter 1, 3, and 6 mm) around the macula, broken into 4 quadrants and 9 sectors

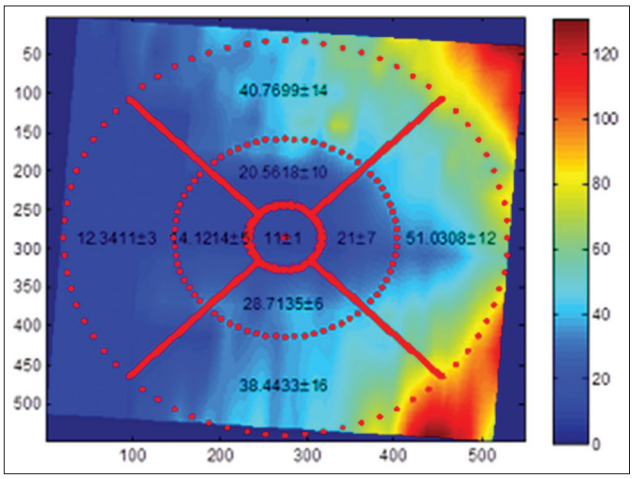

Figure 13: A sample of rotated version of the thickness map for the first layer (retinal nerve fiber layer)

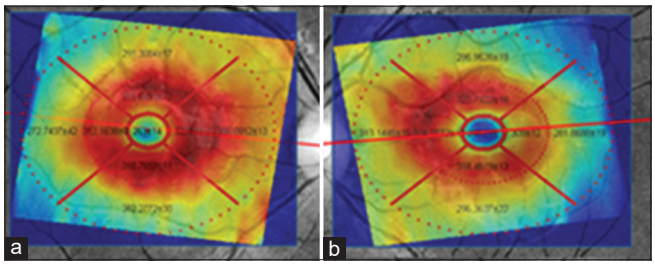

Figure 14: Optical coherence tomography thickness map and fundus in both eyes after registration. (a) Right eye, (b) left eye

(the tolerance limit). To follow this hypothesis, we showed that the normal plot of the mean differences in each sector of retinal layers is almost linear and can be considered as a proof for its Gaussian distribution [Figure 15].

Results

In order to have a quantitative measure of the symmetry between the right and left eyes, the mean thickness difference (right thickness minus left thickness) in each

Table 4: Absolut normal tolerance limits mean±(2×standard deviation) in thickness of retinal layers

Layer	Sector 1	Sector 2	Sector 3	Sector 4	Sector 5	Sector 6	Sector 7	Sector 8	Sector 9
1th	1.15±(2×0.95)	2.64±(2×1.54)	4.16±(2×1.89)	1.23±(2×1.45)	2.68±(2×1.40)	4.03±(2×1.56)	4.86±(2×3.18)	2.36±(2×1.67)	3.65±(2×1.39)
2nd	6.87±(2×2.69)	6.09±(2×3.09)	8.49±(2×3.58)	7.16±(2×4.41)	8.97±(2×3.06)	6.88±(2×3.15)	8.48±(2×3.53)	6.46±(2×2.89)	9.29±(2×3.37)
3rd	7.94±(2×2.10)	5.28±(2×1.78)	5.55±(2×1.98)	5.33±(2×1.85)	5.14±(2×2.89)	5.60±(2×2.70)	6.33±(2×2.85)	3.37±(2×2.18)	7.63±(2×3.02)
4th	7.769±(2×2.48)	5.28±(2×2.92)	5.97±(2×3.39)	5.06±(2×3.55)	5.46±(2×4.32)	4.04±(2×2.65)	6.69±(2×4.74)	4.17±(2×3.14)	8.59±(2×4.39)
5th	3.27±(2×1.72)	2.97±(2×0.99)	1.68±(2×1.72)	2.49±(2×1.32)	2.81±(2×0.99)	1.73±(2×0.60)	1.83±(2×0.94)	2.06±(2×0.81)	1.27±(2×1.05)
6th	6.31±(2×2.66)	4.07±(2×1.58)	4.07±(2×1.58)	5.55±(2×3.22)	4.28±(2×2.36)	4.07±(2×2.44)	4.93±(2×4.78)	4.99±(2×4.74)	8.70±(2×4.02)
7th	1.19±(2×1.09)	0.417±(2×0.2)	0.71±(2×0.76)	1.72±(2×1.95)	0.94±(2×1.04)	0.38±(2×0.64)	1.33±(2×2.48)	1.77±(2×3.56)	0.27±(2×1.24)
8th	1.27±(2×0.63)	0.60±(2×0.38)	0.68±(2×0.47)	0.61±(2×0.28)	0.76±(2×0.29)	0.65±(2×0.42)	0.86±(2×0.97)	0.81±(2×1.43)	0.47±(2×0.66)
9th	0.60±(2×0.28)	0.518±(2×0.1)	0.46±(2×0.19)	0.40±(2×0.20)	0.42±(2×0.15)	0.28±(2×0.19)	0.49±(2×0.52)	0.37±(2×0.60)	0.48±(2×0.32)
10th	0.91±(2×0.50)	0.68±(2×0.36)	0.61±(2×0.39)	0.53±(2×0.34)	0.67±(2×0.33)	0.45±(2×0.27)	0.44±(2×0.73)	0.49±(2×0.60)	0.69±(2×0.44)
11th	1.59±(2×0.72)	1.28±(2×0.48)	0.90±(2×0.59)	1.14±(2×0.52)	0.81±(2×0.43)	0.78±(2×0.56)	1.54±(2×1.46)	1.02±(2×1.80)	0.92±(2×1.10)
Total retina	10.72±(2×3.04)	3.62±(2×3.05)	5.22±(2×3.39)	4.11±(2×2.85)	6.83±(2×4.83)	7.04±(2×3.68)	12.73±(2×18.8)	9.26±(2×19.9)	10.27±(2×10.2)

Sector 1 – Fovea; Sector 2 – Parafoveal nasal; Sector 3 – Parafoveal inferior; Sector 4 – Parafoveal temporal; Sector 5 – Parafoveal superior; Sector 6 – Perifoveal nasal; Sector 7 – Perifoveal inferior; Sector 8 – Perifoveal temporal; Sector 9 – Perifoveal superior

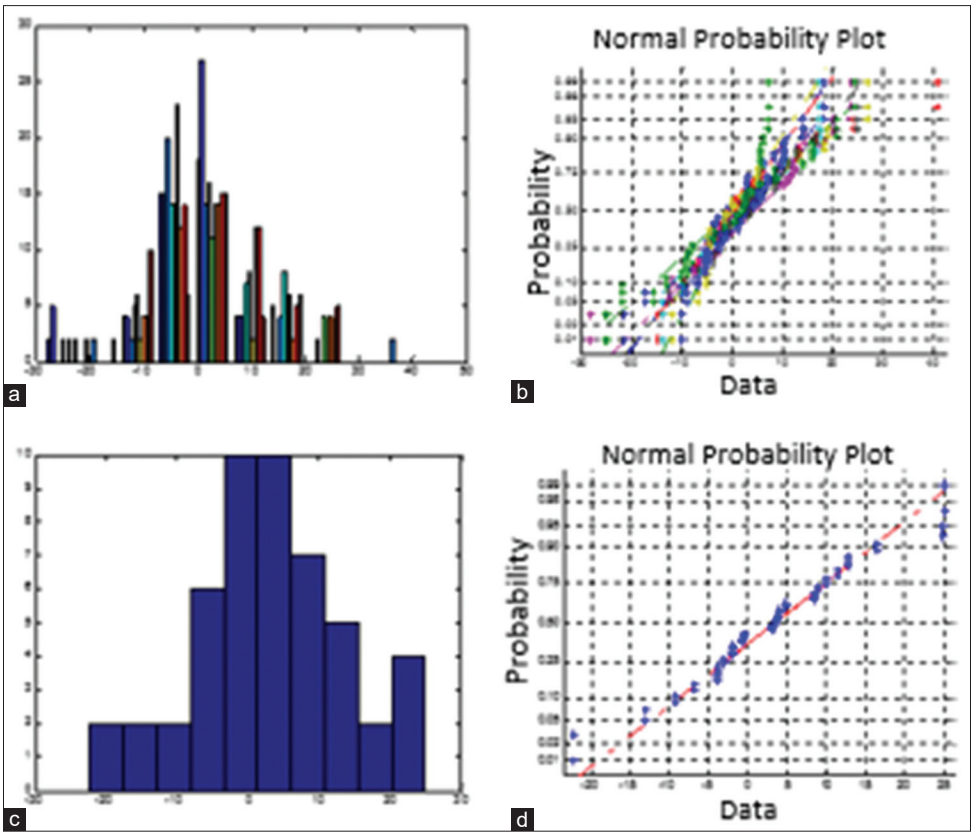

Figure 15: (a) Histogram showing the frequency distribution of the differences in mean for one layer. (b) Normal probability plot for one layer. (c) Histogram showing the frequency distribution of the differences in mean for one sector of layer. (d) Normal probability plot for one sector of layer

Table 5: *P* values of the differences

Layers	Sector 1	Sector 2	Sector 3	Sector 4	Sector 5	Sector 6	Sector 7	Sector 8	Sector 9
1st layer	0.005	0.36	0.35	0.20	0.49	0.34	0.35	0.02	0.40
2nd layer	0.42	0.41	0.19	0.29	0.35	0.33	0.18	0.35	0.33
3rd layer	0.27	0.21	0.45	0.49	0.35	0.22	0.18	0.37	0.30
4th layer	0.05	0.36	0.05	0.15	0.23	0.48	0.45	0.37	0.18
5th layer	0.05	0.49	0.28	0.04	0.34	0.48	0.48	0.41	0.45
6th layer	0.05	0.31	0.05	0.01	0.07	0.30	0.26	0.05	0.48
7th layer	0.24	0.41	0.26	0.005	0.14	0.20	0.16	0.37	0.48
8th layer	0.32	0.50	0.29	0.45	0.38	0.33	0.43	0.23	0.32
9th layer	0.40	0.42	0.36	0.36	0.25	0.46	0.45	0.37	0.41
10th layer	0.45	0.46	0.42	0.46	0.47	0.42	0.48	0.32	0.28
11th layer	0.34	0.44	0.39	0.45	0.44	0.34	0.42	0.47	0.37
Total retina thickness	0.17	0.31	0.15	0.33	0.34	0.11	0.37	0.26	0.42

Sector 1 – Fovea; Sector 2 – Parafoveal nasal; Sector 3 – Parafoveal inferior; Sector 4 – Parafoveal temporal; Sector 5 – Parafoveal superior; Sector 6 – Perifoveal nasal; Sector 7 – Perifoveal inferior; Sector 8 – Perifoveal temporal; Sector 9 – Perifoveal superior

layer is investigated for 9 sectors around the macula. The maximum and minimum of the thickness for each layer of two eyes are shown in Table 3. Furthermore, Table 4 summarizes the absolute normal tolerance limits. For instance, tolerance limits in RNFL thickness for 9 sectors are 1.15± (2 × 0.95) in sector 1, 2.64± (2 × 1.54) in sector 2, 4.16± (2 × 1.89) in sector 3, 1.23± (2 × 1.45) in sector 4, 2.68± (2 × 1.40) in sector 5, 4.03± (2 × 1.56) in sector 6, 4.86± (2 × 3.18) in sector 7, 2.36± (2 × 1.67) in sector 8, and 3.65± (2 × 1.39) in sector 9 (in μm). To justify the significance of the obtained differences, *P* value is also obtained for each layer in Table 5. *P* value indicates asymmetry on RNFLT in fovea and perifoveal temporal sectors between two eyes ($P < 0.05$). We also showed the detailed results for a sample layer (6th layer) in Table 6.

Conclusion

The present study is set to determine normal tolerance limits for asymmetry of inter-retinal layers' thickness in normal population. Knowing the tolerance limits,

Table 6: The detailed results of asymmetry analysis on a sample layer (6th layer)

Sector	Mean±SD (μm)		Unsigned mean±SD of differences (μm)	*P*
	Right eye	Left eye		
1. Fovea	78.79±6.04	81.08±4.90	6.31±(2×2.66)	0.05
2. Parafoveal nasal	73.05±5.26	73.77±5.28	4.07±(2×1.58)	0.31
3. Parafoveal inferior	69.69±7.09	72.89±6.47	5.52±(2×2.75)	0.05
4. Parafoveal temporal	67.76±6.90	71.22±4.18	5.55±(2×3.22)	0.01
5. Parafoveal superior	69.08±5.30	71.24±4.94	4.28±(2×2.36)	0.07
6. Perifoveal nasal	63.86±7.58	65.02±8.03	4.07±(2×2.44)	0.30
7. Perifoveal inferior	56.18±9.76	58.07±10.82	4.93±(2×4.78)	0.26
8. Perifoveal temporal	56.43±11.43	61.12±7.99	4.99±(2×4.74)	0.050
9. Perifoveal superior	61.64±7.18	61.72±9.31	8.70±(2×4.02)	0.48

SD – Standard deviation

we may suspect when patients would exceed these limits.

The state of being or not being asymmetric in retinal layers' thickness is investigated for the first time in this article. The results show that most of the sectors in each retinal layer are not significantly asymmetry, but some specific sectors of retinal layers have significant asymmetry with $P < 0.05$ in normal population. Fifth to seventh layer and RNFL seem to be more tedious to be asymmetric. Perifoveal and parafoveal temporal sectors and ventral fovea sector are more asymmetric in comparison with other sectors.

We also determined normal tolerance limits for asymmetry of retinal layer thickness in normal population. The normal tolerance limit has the highest value in perifoveal inferior, suggesting that the asymmetric values in this region are not a reliable sign of abnormalities. On the other hand, parafoveal nasal sector has a narrow normal limit of asymmetry and small variations in this region should be considered as a possible sign of abnormal situation.

One of the limitations in this work is the correct localization of the fovea on OCT projections. The incorrect location can alter the results considerably since many stages are dependent on it. Two potential sources of error are manual determination of the convolution templates, and the use of convolution operator on these templates, which leads to an error of 20.51 ± 6.09 μm in this research. A possible alternate to this method is localization of fovea using the deepest point in internal limiting membrane surface. This might be an accurate method supposing that dense OCT scans are available. To clear up, in this work, 128 scans provide a resolution of 46.88 × 11.72 μm/pixel. Namely, each B-scan is located 46.88 μm far from the next B-scan. In most fortunate conditions, one B-scan passes from the fovea and the deepest point would lead correctly to the result; otherwise, an error of at most 23.44 = 46.88/2 μm would be expected. This becomes worse if the number of scans would reduce to common numbers like 20 scans. We, therefore, admitted the convolution strategy with calculated 20.51 ± 6.09 μm error. This might be trivial comparing with 23.44 = 46.88/2 μm error in 128-slice acquisition but is considerably low in other datasets with low number of slices.

In conclusion, this article shows that normal population does not have identical retinal information in both eyes, and without considering this reality, normal asymmetry in information gathered from both eyes might be interpreted as retinal disorders.

We are now working on developing this study for evaluating asymmetry/symmetry in patients suffering from different ocular diseases. Furthermore, other features such as cup-to-disc ratio using ONH OCT may be considered in symmetry analysis in future works.

Acknowledgment

The authors would like to thank Ms. A. Soltanipour *et al.* for providing the source code of vessel segmentation.

Financial support and sponsorship

None.

Conflicts of interest

There are no conflicts of interest.

References

1. Ghorbel I, Rossant F, Bloch I, Tick S, Paques MJ. Automated segmentation of macular layers in OCT images and quantitative evaluation of performances. Pattern Recognition 2011;44:1590-603.
2. Garvin MK, Abramoff MD, Kardon R, Russell SR, Wu X, Sonka M. Intraretinal layer segmentation of macular optical coherence tomography images using optimal 3-D graph search. IEEE Trans Med Imaging 2008;27:1495-505.
3. Quellec G, Lee K, Dolejsi M, Garvin MK, Abràmoff MD, Sonka M. Three-dimensional analysis of retinal layer texture: Identification of fluid-filled regions in SD-OCT of the macula. IEEE Trans Med Imaging 2010;29:1321-30.
4. Asrani S, Rosdahl JA, Allingham RR. Novel software strategy for glaucoma diagnosis: Asymmetry analysis of retinal thickness. Arch Ophthalmol 2011;129:1205-11.
5. Huynh SC, Wang XY, Burlutsky G, Mitchell P. Symmetry of optical coherence tomography retinal measurements in young children. Am J Ophthalmol 2007;143:518-20.
6. Kurimoto Y, Matsuno K, Kaneko Y, Umihira J, Yoshimura N.

Asymmetries of the retinal nerve fibre layer thickness in normal eyes. Br J Ophthalmol 2000;84:469-72.
7. Essock EA, Sinai MJ, Fechtner RD. Interocular symmetry in nerve fiber layer thickness of normal eyes as determined by polarimetry. J Glaucoma 1999;8:90-8.
8. Mwanza JC, Durbin MK, Budenz DL; Cirrus OCT Normative Database Study Group. Interocular symmetry in peripapillary retinal nerve fiber layer thickness measured with the Cirrus HD-OCT in healthy eyes. Am J Ophthalmol 2011;151:514-210.
9. Park JJ, Oh DR, Hong SP, Lee KW. Asymmetry analysis of the retinal nerve fiber layer thickness in normal eyes using optical coherence tomography. Korean J Ophthalmol 2005;19:281-7.
10. Budenz DL. Symmetry between the right and left eyes of the normal retinal nerve fiber layer measured with optical coherence tomography (an AOS thesis). Trans Am Ophthalmol Soc 2008;106:252-75.
11. Larsson E, Eriksson U, Alm A. Retinal nerve fibre layer thickness in full-term children assessed with Heidelberg retinal tomography and optical coherence tomography: Normal values and interocular asymmetry. Acta Ophthalmol 2011;89:151-8.
12. Altemir I, Oros D, Elía N, Polo V, Larrosa JM, Pueyo V. Retinal asymmetry in children measured with optical coherence tomography. Am J Ophthalmol 2013;156:1238-430.
13. Al-Haddad C, Antonios R, Tamim H, Noureddin B. Interocular symmetry in retinal and optic nerve parameters in children as measured by spectral domain optical coherence tomography. Br J Ophthalmol 2014;98:502-6.
14. Dalgliesh JD, Tariq YM, Burlutsky G, Mitchell P. Symmetry of retinal parameters measured by spectral-domain OCT in normal young adults. J Glaucoma 2015;24:20-4.
15. Alluwimi MS, Swanson WH, Malinovsky VE. Between-subject variability in asymmetry analysis of macular thickness. Optom Vis Sci 2014;91:484-90.
16. Mahmudi T, Kafieh R, Rabbani H, Mehri A, Akhlagi M, editors. Asymmetry evaluation of Fundus Images in Right and Left Eyes Using Radon Transform and Fractal Analysis. Image Processing (ICIP), 2015 IEEE International Conference on; 2015.
17. Mahmudi T, Kafieh R, Rabbani H, Akhlagi M, editors. Comparison of macular OCTs in right and left eyes of normal people. Medical Imaging 2014: Biomedical Applications in Molecular, Structural, and Functional Imaging: International Society for Optics and Photonics; 2014.
18. Hwang YH, Song M, Kim YY, Yeom DJ, Lee JH. Interocular symmetry of retinal nerve fibre layer thickness in healthy eyes: A spectral-domain optical coherence tomographic study. Clin Exp Optom 2014;97:550-4.
19. Lee SY, Jeoung JW, Park KH, Kim DM. Macular ganglion cell imaging study: Interocular symmetry of ganglion cell-inner plexiform layer thickness in normal healthy eyes. Am J Ophthalmol 2015;159:315-2300.
20. Dalgliesh JD, Tariq YM, Burlutsky G, Mitchell P. Symmetry of retinal parameters measured by spectral-domain OCT in normal young adults. J Glaucoma 2015;24:20-4.
21. Zhou M, Lu B, Zhao J, Wang Q, Zhang P, Sun X. Interocular Symmetry of Macular Ganglion Cell Complex Thickness in Young Chinese Subjects. PLoS One 2016;11:e0159583.
22. Yang M, Wang W, Xu Q, Tan S, Wei S. Interocular symmetry of the peripapillary choroidal thickness and retinal nerve fibre layer thickness in healthy adults with isometropia. BMC Ophthalmol 2016;16:182.
23. Lee SY, Lee EK, Park KH, Kim DM, Jeoung JW. Asymmetry analysis of macular inner retinal layers for glaucoma diagnosis: Swept-source optical coherence tomography study. PLoS One 2016;11:e0164866.
24. Yamada H, Hangai M, Nakano N, Takayama K, Kimura Y, Miyake M, *et al*. Asymmetry analysis of macular inner retinal layers for glaucoma diagnosis. Am J Ophthalmol 2014;158:1318-29. e3.
25. Mokhtari M, Rabbani H, Mehri-Dehnavi A, Kafieh R, Akhlaghi MR, Pourazizi M, *et al*. Local comparison of cup to disc ratio in right and left eyes based on fusion of color fundus images and OCT B-scans. Inf Fusion 2019;51:30-41.
26. Liao R, Zhang L, Sun Y, Miao S, Chefd'Hotel C. A review of recent advances in registration techniques applied to minimally invasive therapy. IEEE Trans Multimedia 2013;15:983-1000.
27. Kafieh R, Rabbani H, Abramoff MD, Sonka M. Intra-retinal layer segmentation of 3D optical coherence tomography using coarse grained diffusion map. Med Image Anal 2013;17:907-28.
28. Kafieh R, Rabbani H, Hajizadeh F, Abràmoff MD, Sonka M. Thickness Mapping of Eleven Retinal Layers in Normal Eyes Using Spectral Domain Optical Coherence Tomography. arXiv: 13123199 [csCV] 2015;2015:1-14.
29. Andersson J. Diffusion Geometry with Applications to Virus Classification: Master Thesis at Dep. Math. Royal Academy of Science, Trita-mat-2008-11; 2008.
30. Neji R, Langs G, Deux J-F, Maatouk M, Rahmouni A, Bassez G, *et al*., editors. Unsupervised Classification of Skeletal Fibers Using Diffusion Maps. Biomedical Imaging: From Nano to Macro, 2009 ISBI'09 IEEE International Symposium on; 2009.
31. Shen X, Meyer FG, editors. Nonlinear Dimension Reduction and Activation Detection for FMRI Dataset. Computer Vision and Pattern Recognition Workshop, 2006 CVPRW'06 Conference on, IEEE; 2006.
32. Kafieh R, Rabbani H, Kermani S. A review of algorithms for segmentation of optical coherence tomography from retina. J Med Signals Sens 2013;3:45-60.
33. Qu G, Zhang D, Yan P. Information measure for performance of image fusion. Electron Lett 2002;38:313-5.
34. Gorczynska I, Srinivasan VJ, Vuong LN, Chen RW, Liu JJ, Reichel E, *et al*. Projection OCT fundus imaging for visualising outer retinal pathology in non-exudative age-related macular degeneration. Br J Ophthalmol 2009;93:603-9.
35. Jalili J, Rabbani H, Akhlaghi M, Kafieh R, Mehridehnavi A, editors. Forming Projection Images from Each Layer of Retina Using Diffusion May Based OCT Segmentation. 2012 11th International Conference on Information Science, Signal Processing and their Applications (ISSPA), IEEE; 2012.
36. Sinthanayothin C, Boyce JF, Cook HL, Williamson TH. Automated localisation of the optic disc, fovea, and retinal blood vessels from digital colour fundus images. Br J Ophthalmol 1999;83:902-10.
37. Sekhar S, Al-Nuaimy W, Nandi AK, editors. Automated Localisation of Retinal Optic Disk Using HOUGH Transform. Biomedical Imaging: From Nano to Macro, 2008 ISBI 2008 5th IEEE International Symposium on; 2008.
38. Ibañez MV, Simó A. Bayesian detection of the fovea in eye fundus angiographies. Pattern Recognit Lett 1999;20:229-40.
39. Chaudhuri S, Chatterjee S, Katz N, Nelson M, Goldbaum M. Detection of blood vessels in retinal images using two-dimensional matched filters. IEEE Trans Med Imaging 1989;8:263-9.
40. Bonanomi MT, Nicoletti AG, Carricondo PC, Buzalaf F, Kara-José N Jr, Gomes AM, *et al*. Retinal thickness assessed by optical coherence tomography (OCT) in pseudophakic macular edema. Arq Bras Oftalmol 2006;69:539-44.

41. Kafieh R, Rabbani H, Abramoff MD, Sonka M. Curvature correction of retinal OCTs using graph-based geometry detection. Phys Med Biol 2013;58:2925-38.
42. Antony BJ, Stetson PF, Abramoff MD, Lee K, Colijn JM, Buitendijk GH, *et al*. Characterizing the impact of off-axis scan acquisition on the reproducibility of total retinal thickness measurements in sdoct volumes. Transl Vis Sci Technol 2015;4:3.
43. Esmaeili M, Rabbani H, Dehnavi AM. Automatic optic disk boundary extraction by the use of curvelet transform and deformable variational level set model. Pattern Recognit 2012;45:2832-42.
44. Alipour SH, Rabbani H, Akhlaghi M, Dehnavi AM, Javanmard SH. Analysis of foveal avascular zone for grading of diabetic retinopathy severity based on curvelet transform. Graefes Arch Clin Exp Ophthalmol 2012;250:1607-14.
45. Soltanipour A, Sadri S, Rabbani H, Akhlaghi M, Doost-Hosseini A, editors. Vessel centerlines extraction from fundus fluorescein angiogram based on hessian analysis of directional curvelet subbands. Acoustics, Speech and Signal Processing (ICASSP), 2013 IEEE International Conference on; 2013
46. Chew EY, Klein ML, Ferris FL 3rd, Remaley NA, Murphy RP, Chantry K, *et al*. Association of elevated serum lipid levels with retinal hard exudate in diabetic retinopathy. Early treatment diabetic retinopathy study (ETDRS) Report 22. Arch Ophthalmol 1996;114:1079-84.

BIOGRAPHIES

Tahereh Mahmoudi received her B.S. degree in Electrical Engineering (Electronic) from Shiraz University (2003) and M.Sc. in biomedical engineering from Isfahan University of Medical Sciences (2013). She is currently PhD student in biomedical engineering at Tehran University of Medical Sciences, Tehran, Iran. Her research interests are in biomedical image analysis, pattern recognition, classification and image segmentation.

Email: t-mahmoudi@razi.tums.ac.ir

Rahele Kafieh received her BSc in Bioelectrical Engineering at Sahand University of Technology (2004) and completed her Msc and PhD in Bioelectrical Engineering at Isfahan University of Medical Sciences (2008 and 2014). She is Assistant Professor at School of Advanced Technologies in Medicine, Isfahan University of Medical Sciences, Isfahan, Iran and guest researcher at Neurocure Clinical Research Center, Charite University, Berlin, Germany. Her research is concentrated on biomedical image analysis, problems in area of graph based image analysis, time-frequency methods, deep learning and image segmentation.

Email: r_kafieh@yahoo.com

Hossein Rabbani received his BSc degree in Electrical Engineering (Communications) from Isfahan University of Technology in 2000 with the highest honors, and his MSc and PhD degrees in Bioelectrical Engineering in 2002 and 2008, respectively, from Amirkabir University of Technology. In 2007 he was with Queen's University, as a Visiting Researcher, in 2011 with University of Iowa, as a Postdoctoral Research Scholar, and in 2013-2014 with Duke University as a Postdoctoral Fellow. He is now a professor in Biomedical Engineering Department and Medical Image & Signal Processing Research Center (MISP), Isfahan University of Medical Sciences, Isfahan, Iran, and Editor in-Chief of Journal of Medical Signals and Sensors (JMSS). His main research interests are medical image analysis and modeling, statistical (m-D) signal processing, sparse transforms, and image restoration.

Email: h_rabbani@med.mui.ac.ir

Alireza Mehri Dehnavi received BSc in Electrical Engineering from Isfahan University of Technology in 1988, MSc of Engineering in Measurement and Instrumentation from Indian Institute of Technology Roorkee in 1992 and PhD in Medical Engineering from Liverpool University in 1996. He is a Professor of Biomedical Engineering in School of Advanced Technologies in Medicine of Isfahan University of Medical Sciences. His research interests are medical optics, devices and signal processing.

Email: mehri@med.mui.ac.ir

Mohammad Reza Akhlaghi is an Associate Professor in Department of Ophthalmology, Isfahan University of Medical Sciences, Isfahan, Iran. He received his VitreoRetinal Fellowship in 2006 from the Tehran University of Medical Sciences.

Email: akhlaghi@med.mui.ac.ir